

## Identification of 14-3-3 $\epsilon$ Substrates from Embryonic Murine Brain

Bryan A. Ballif,<sup>\*,†</sup> Zhongwei Cao,<sup>‡</sup> Daniel Schwartz,<sup>†</sup> Kermit L. Carraway III,<sup>‡</sup> and Steven P. Gygi<sup>\*,†</sup>

*Department of Cell Biology, Harvard Medical School, 240 Longwood Avenue, Boston, Massachusetts 02115, and University of California at Davis Cancer Center, 4645 2nd Avenue, Sacramento, California 95817*

Received May 2, 2006

Mice deficient in 14-3-3 $\epsilon$  exhibit abnormal neuronal migration and die perinatally. We report here the first large-scale analysis of 14-3-3 interacting partners from primary animal tissue, identifying from embryonic murine brain 163 14-3-3 $\epsilon$  interacting proteins and 85 phosphorylation sites on these proteins. Phosphorylation of the deubiquitinating enzyme USP8 at serine 680 was found essential for its interaction with 14-3-3 $\epsilon$  and for maintaining USP8 in the cytosol.

**Keywords:** phosphoproteomics • 14-3-3 • epsilon • brain development • kinase • phosphorylation • mass spectrometry • deubiquitination

### Introduction

Proper development of the mammalian brain requires nascent neurons to be positioned in distinct interdependent spatial patterns. Correct neuronal positioning is largely accomplished through attractive and repulsive molecular guidance cues that instruct neurons to migrate or extend processes over sometimes great distances. The mammalian cerebral cortex is layered through successive rounds of radial migration out toward the pial surface from proliferation-competent ventricular zones (VZs)<sup>1</sup>. Balanced asymmetric cell division renews the proliferation potential of VZs and simultaneously generates appropriate numbers of post-mitotic migratory neurons. Disrupting this balance has severe consequences during cortex formation. The early generation of too many migratory neurons can prematurely deplete proliferative cells leading to too few migratory neurons at later stages. Conversely, the generation of too few migratory neurons could inappropriately delay or diminish cortical layering. This balance was recently shown to be maintained through Nde1 (mNudE)-dependent orientation and regulation of the mitotic spindle in ventricular proliferative cells.<sup>2</sup>

In addition to correct mitotic regulation in VZs, cortical development relies on migratory neurons to be equipped with appropriately wired signal transduction circuits and competent intracellular effector machines which work together to drive changes in cellular architecture and mobility. Loss of signal transduction machinery, as in deficiencies in Reelin/Disabled-1 (Dab1) signaling or cyclin-dependent kinase 5 (Cdk5) activity, leads to cortical layering defects.<sup>3,4</sup> Little is known about how Reelin/Dab1 signaling alters neuronal positioning, although it

might regulate cell adhesion by recruiting a Crk(L)/C3G/Rap1 signaling complex to phosphorylated Dab1.<sup>5</sup> A growing number of Cdk5 substrates have been identified, and recent work has shown Cdk5 phosphorylates Ndel1 (NUDEL), an essential regulator of nuclear translocation (nucleokinesis).<sup>6,7</sup> Nucleokinesis requires Ndel1-dependent regulation of the molecular motor, cytoplasmic dynein, which is responsible for pulling the nucleus along the microtubule network.<sup>8</sup> Cdk5 phosphorylation of Ndel1 creates binding sites for 14-3-3 $\epsilon$ , and these sites are essential for proper subcellular localization of Ndel1 and cytoplasmic dynein.<sup>6</sup>

The 14-3-3 protein family executes diverse regulatory roles primarily via interactions with proteins phosphorylated in conserved sequence motifs.<sup>9,10</sup> Mice deficient in 14-3-3 $\epsilon$  have neuronal migration defects during cortical development despite the expression of multiple mammalian 14-3-3 isoforms in the developing brain.<sup>6</sup> In addition, human patients with lissencephalies due to haploinsufficiencies of LIS1, another regulator of cytoplasmic dynein, have a more severe phenotype when they are also haploinsufficient in either 14-3-3 $\epsilon$  or Crk.<sup>11</sup> 14-3-3 family members are thought to function as homo- and heterodimers,<sup>12</sup> and it is thus anticipated that 14-3-3 $\epsilon$  may effectively bridge substrates that may otherwise never interact. Given the potential for great diversity in 14-3-3 $\epsilon$  substrate complexes, we sought to identify from the developing murine brain additional substrates of 14-3-3 $\epsilon$  that might regulate the molecular machinery of proliferative as well as migratory neurons.

Four independent studies have previously reported the large-scale identification of mammalian substrates for different 14-3-3 isoforms.<sup>13–16</sup> Using affinity chromatography, Pozuelo Rubio et al. identified more than 200 substrates of the two *Saccharomyces cerevisiae* 14-3-3 isoforms (BMH1 and BMH2) from asynchronous HeLa extracts,<sup>13</sup> and Meek et al. identified more than 300 14-3-3 $\zeta$  substrates from asynchronous and mitotic HeLa cell extracts.<sup>14</sup> Jin et al. employed immunoaffinity purification using an epitope-tagged 14-3-3 $\gamma$  HEK 293 stable cell

\* Corresponding authors: Bryan A. Ballif, Ph.D. Current address: 109 Carrigan Drive, Department of Biology, University of Vermont, Burlington, VT, 05405. Tel: (802) 656-2922. Fax: (802) 656-2914. Steven P. Gygi, Ph.D., Department of Cell Biology, Harvard Medical School, 240 Longwood Avenue, Boston, MA 02115. Tel: (617) 432-3154. Fax: (617) 432-1144.

<sup>†</sup> Harvard Medical School.

<sup>‡</sup> University of California at Davis Cancer Center.

line and identified 170 substrates,<sup>15</sup> and Benzinger et al. applied a similar strategy to identify 117 binding partners of 14-3-3 $\sigma$ .<sup>16</sup> As 14-3-3 $\epsilon$  plays a specific role in corticogenesis, we sought to identify 14-3-3 $\epsilon$  phosphoprotein substrates that are expressed in the developing brain itself and to determine if they overlap with substrates identified for other 14-3-3 isoforms using immortalized cell lines.

## Experimental Procedures

**Plasmids and Antibodies.** pGEX-4T-14-3-3 $\epsilon$  (rat) wild-type and K49E were gifts of M. Yaffe and have been described previously.<sup>9</sup> V5-tagged USP8 (mouse) full-length, T3 and T8 constructs in pCDNA3.1+ were described previously,<sup>17</sup> and the S680A mutant was generated by the quick-change method (Stratagene, La Jolla, CA). Antibodies were from the following sources:  $\alpha$ -V5 (Invitrogen, Carlsbad, CA),  $\alpha$ -phospho-14-3-3 substrate (Cell Signaling Technology, Beverly, MA), and  $\alpha$ -Ndel1 (NUDEL) was a gift of S. Hirotsune (Osaka City University, Osaka, Japan).

**Purification of 14-3-3 $\epsilon$  Interacting Partners from Embryonic Brain Extract.** Timed pregnant Swiss Webster mice were ordered from Taconic (Germantown, NY), and embryonic brains were extracted at day 16.5 (E16.5). The forebrains and midbrains from 57 embryos were combined and dounce-homogenized in protein complex lysis buffer (PCLB) composed of 25 mM Tris, pH 7.4, 137 mM NaCl, 1% NP-40, 10% glycerol, 25 mM NaF, 10 mM Na<sub>4</sub>P<sub>2</sub>O<sub>7</sub>, 1 mM Na<sub>3</sub>VO<sub>4</sub>, 1 mM DTT, 1 mM PMSF, 10  $\mu$ g/mL leupeptin, and 1% aprotinin. Cellular debris was pelleted by centrifugation for 30 min at 15 000g. The supernatant, corresponding to 145 mg of protein, was pre-cleared to reduce nonspecific binding proteins over 350  $\mu$ L of packed glutathionine sepharose (GE/Amersham/Pharmacia, Piscataway, NJ), and then was further cleared by pouring it sequentially over glutathione-sepharose columns bound to 500  $\mu$ g of GST and 350  $\mu$ g of GST-14-3-3 $\epsilon$  K49E, respectively. The flow-through was divided equally and poured over either a second GST-14-3-3 $\epsilon$  K49E column (250  $\mu$ g) or a column of GST-14-3-3 $\epsilon$  wild-type (250  $\mu$ g) (Figure 1). These final columns were washed with 30 mL of PCLB, and then 10 mL of 50 mM HEPES, pH 7.4, 137 mM NaCl. Embryonic brain proteins bound to each column were eluted stepwise with 400  $\mu$ L of 0.4 M MgCl<sub>2</sub> in 50 mM HEPES, 400  $\mu$ L of 0.8 M MgCl<sub>2</sub> in 50 mM HEPES, and finally chased with 200  $\mu$ L of 50 mM HEPES. Eluates were combined and precipitated with 15% trichloroacetic acid. Precipitated proteins were pelleted, washed with acetone, resuspended in sample buffer, pH-adjusted with 1/6 volume of 1 M Tris base, boiled, and subjected to SDS-PAGE on a 10% (37.5:1 acrylamide/bis-acrylamide) gel which was either stained with coomassie or subjected to immunoblotting. Prior to this larger-scale experiment the same was performed using 30 mg of embryonic brain extract with similar results based on silver-staining of TCA precipitates separated by SDS-PAGE (data not shown).

**In-Gel Digestion and Mass Spectrometry.** Gel bands and regions (Supporting Information Figure 1) were cut into 1 mm cubes, washed with water, and destained with 50% acetonitrile (MeCN) and 50 mM NH<sub>4</sub>HCO<sub>3</sub>, pH 8.5. Gel pieces were fully dehydrated with MeCN, dried, and then allowed to swell on ice with 12.5 ng/ $\mu$ L of sequencing-grade modified trypsin (Promega, Madison, WI) in 50 mM NH<sub>4</sub>HCO<sub>3</sub>, pH 8.5. After swelling, an equal volume of 50 mM NH<sub>4</sub>HCO<sub>3</sub> was added, and in-gel digestion was allowed to proceed overnight at 37  $^{\circ}$ C. Peptides were extracted with 50% MeCN and 2.5% formic acid

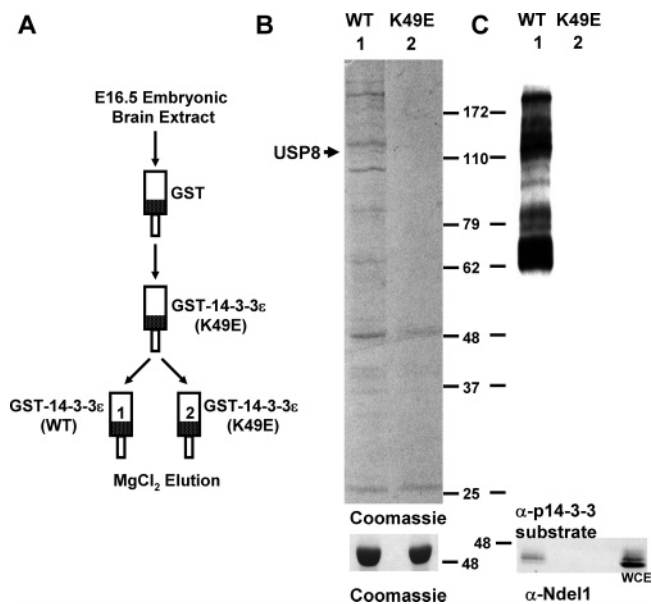


**Figure 1.** Identification of 14-3-3 $\epsilon$  interacting proteins from murine embryonic brain. (A) Embryonic brain extract was subjected to a subtractive chromatography strategy to enrich for phospho-dependent 14-3-3 $\epsilon$  binding partners. After passing the extract sequentially over a column of GST and GST-14-3-3 $\epsilon$  (K49E), the flow-through was divided in half and applied in parallel to another column of GST-14-3-3 $\epsilon$  (K49E) or GST-14-3-3 $\epsilon$  wild-type. Bound proteins were eluted with MgCl<sub>2</sub> and subjected to SDS-PAGE and coomassie-staining (B) or immunoblotting with an antibody that recognizes the 14-3-3 mode1 binding motif (C). The lower panel in (B) shows proportional amounts of the GST-14-3-3 $\epsilon$  baits in the final two columns after the columns were stripped with hot SDS-PAGE sample buffer. The lower panel in (C) shows the presence of Ndel1 exclusively in the wild-type eluate.

(FA) and dried. Peptides were resuspended in 2.5% MeCN, 2.5% FA and loaded onto a 100  $\mu$ m inner diameter microcapillary column packed with 12 cm of reverse-phase MagicC18 material as described previously.<sup>18</sup> After a 15 min isocratic loading in 2.5% MeCN, 0.15% FA (Solvent A) peptides were eluted using a 4%–35% gradient of Solvent B (95% MeCN, 0.15% FA) over 30 min and electrosprayed into a LCQ-Deca ion trap mass spectrometer (Thermo Electron, San Jose, CA). The precursor scan was followed by collision-induced dissociation (CID) tandem mass spectra for the top 10 most abundant ions. Tandem mass spectra were searched against the mouse IPI database using SEQUEST requiring fully tryptic peptides, allowing a mass tolerance of 2 Da and a mass addition of 80 Da for serine, threonine, and tyrosine residues. The SEQUEST option to consider phosphorylation-dependent neutral loss ions when calculating Xcorr scores was turned off. SEQUEST matches in the first position were then filtered by Xcorr scores of 1.8, 2, and 2.7 for singly, doubly, and triply charged ions, respectively. Protein matches made with more than two peptides were further considered. When such filters were applied to the data searched against the composite forward and reverse mouse IPI databases,<sup>19</sup> no reverse hits remained. This list was then relieved of keratin and trypsin as well as desmoplakin, junction plakoglobin, and titin which were identified in multiple bands throughout the gel and can be common contaminants. The remaining proteins were allowed to include peptides with Xcorr scores of 1.5, 1.8, and 2 for singly,

doubly, and triply charged species, respectively. Given their high occurrence of identification in proteomic experiments, we placed tubulins, actins, myosins, and the t-complex protein chaperones in Supporting Information Table 2, and these proteins were not used in motif analyses. When proteins were identified by only two or three unique peptides, spectra for these peptides were examined manually. This final list was then relieved of all Xcorr cutoffs and filtered for phosphopeptides. The spectrum for each identified phosphopeptide was examined manually for proper phosphorylation site assignment or potential ambiguity. Every identified phosphopeptide is included in Supporting Information Table 1, and any ambiguity in the specific site of phosphorylation is noted. A complete list of unique, unambiguous phosphopeptides is given in Supporting Information Table 3. Tandem mass spectra for all phosphopeptides can be obtained at <http://gygi.med.harvard.edu/pubs/1433/> where hyperlinks to the MS/MS spectra can be downloaded from Supporting Information Table 1.

**Cell Culture, Transfections, and Cell Lysis.** E1A-transformed Human Embryonic Kidney (HEK) 293 cells were used for pulldowns, and COS-7 cells were used for immunofluorescence. Both were cultured in DMEM (Mediatech, Herndon, VA) with 10% heat-inactivated fetal bovine serum (FBS) (Hyclone, Logan, UT) and 50 units/mL penicillin and 50  $\mu$ g/mL streptomycin. Transfection of HEK 293 cells was by calcium phosphate precipitation, and transfection of COS-7 cells was by Fugene6 (Roche, Indianapolis, IN). HEK 293 cell extracts were prepared by washing cells with ice-cold phosphate-buffered saline (PBS) prior to lysis in PCLB. Lysates were centrifuged at 15 000g for 20 min, and the supernatant was subjected to either pulldown assays or immunoblotting directly.

**Pulldown Assays and Immunoblotting.** For pulldowns, whole cell extract was rotated at 4 °C for 2–4 h in batch format with equal amounts of GST-14-3-3 $\epsilon$  wild-type or K49E bound to glutathione sepharose as indicated. Pulldowns were washed three times with PCLB and then subjected to SDS-PAGE and immunoblotting. Immunoblotting was performed on nitrocellulose membranes, and blocking was carried out in 5% instant milk, Tris-buffered saline with 0.05% Tween-20 (TBST), 5 mM NaF, and 1 mM Na<sub>3</sub>VO<sub>4</sub> for 1 h. Primary antibody incubation was performed for 2–4 h in 3% BSA, TBST, 5 mM NaF, 1 mM Na<sub>3</sub>VO<sub>4</sub>, and 0.005% NaN<sub>3</sub>. After four, 10-min TBST washes, HRP-conjugated secondary antibodies (Santa Cruz Biotechnology, Inc., Santa Cruz, CA) were added in TBST for 1 h followed by four more, 10-min TBST washes and detection by enhanced chemiluminescence and exposure to X-ray film.

**Microscopy, Immunofluorescence, and Quantification of USP8 Nuclear Localization.** Indirect immunofluorescence of transfected V5-tagged USP8 constructs in COS-7 cells was carried out with cells fixed on cover slips as previously described,<sup>20</sup> using AlexaFluor 488-labeled secondary antibody (Molecular Probes, Eugene, OR) to visualize V5-USP8 localization and DAPI to visualize the nucleus. To quantify nuclear localization, 50–70 transfected cells over several fields were scored for whether AlexaFluor 488 staining was detected in the nucleus. The experiment was performed three times with similar results. Figure 5 shows the data for one representative experiment.

**Phospho-Based and Protein-Based Motif Analyses.** Motif extraction was carried out using the motif-x software via its online server (<http://motif-x.med.harvard.edu>). This software employs an iterative statistically based motif extraction algorithm as previously described.<sup>21</sup> In the case of the MS/MS-based

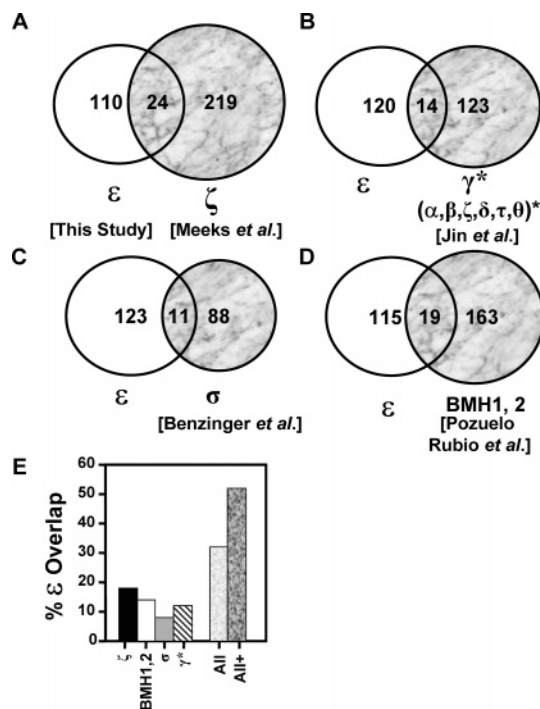


**Figure 2.** Comparison of 14-3-3 $\epsilon$  interacting proteins identified in this study with those found in the four other proteomic studies using different 14-3-3 isoforms. Venn diagrams (A–D) show the overlap of 14-3-3 $\epsilon$  interacting proteins with other 14-3-3 isoforms. Toward a normalized comparison, major structural proteins such as tubulins, actins, and keratins, as well as hypothetical or unnamed proteins were removed from the list prior to creation of the Venn diagrams. The precise proteins used to create the Venn diagrams and those unique to this study are presented in Supporting Information Tables 5 and 6, respectively. (E) Bar graphs showing the percent of 14-3-3 $\epsilon$  interacting proteins found to interact with other 14-3-3 isoforms in mammalian proteomic experiments are as indicated. “All” denotes the percent overlap of 14-3-3 $\epsilon$  interacting proteins with all of the proteins identified in the four studies combined. “All+” shows the overlap if the four proteomic studies found 14-3-3 interacting proteins that were isoforms of but different from the 14-3-3 $\epsilon$  interacting proteins identified in this study (see text for further details). \*In the study conducted by Jin and colleagues, initial smaller experiments were conducted with 14-3-3 isoforms  $\alpha$ ,  $\beta$ ,  $\zeta$ ,  $\delta$ ,  $\tau$ , and  $\theta$  before their larger study with 14-3-3 $\gamma$ . To be as inclusive as possible, the comparison is made with the sum of the interacting proteins they identified using each isoform.

phosphorylation data set, unambiguous, nonredundant tryptic phosphoserine-containing peptides ( $n = 62$ ) were submitted to the motif-x server using the “MS/MS” option and the parameters central character = S\* (the “\*” symbol denoted phosphorylated residues in our data set), width = 13, occurrences = 10, significance  $\leq 10^{-6}$ , and background = IPI mouse proteome. The “MS/MS” option extended the peptides N- and C-terminally so as to retrieve at least 6 residues upstream and downstream of each phosphorylation site. For the motif analysis of 14-3-3 $\epsilon$  interacting proteins ( $n = 163$ ), a file containing these protein sequences was uploaded to the motif-x server using the FASTA option with the following parameters: width = 13, occurrences = 20, and significance  $\leq 10^{-6}$ . The central residue parameter was varied for all 20 possible residues. The background parameter was set at either “unaligned foreground” or “IPI mouse proteome” with similar

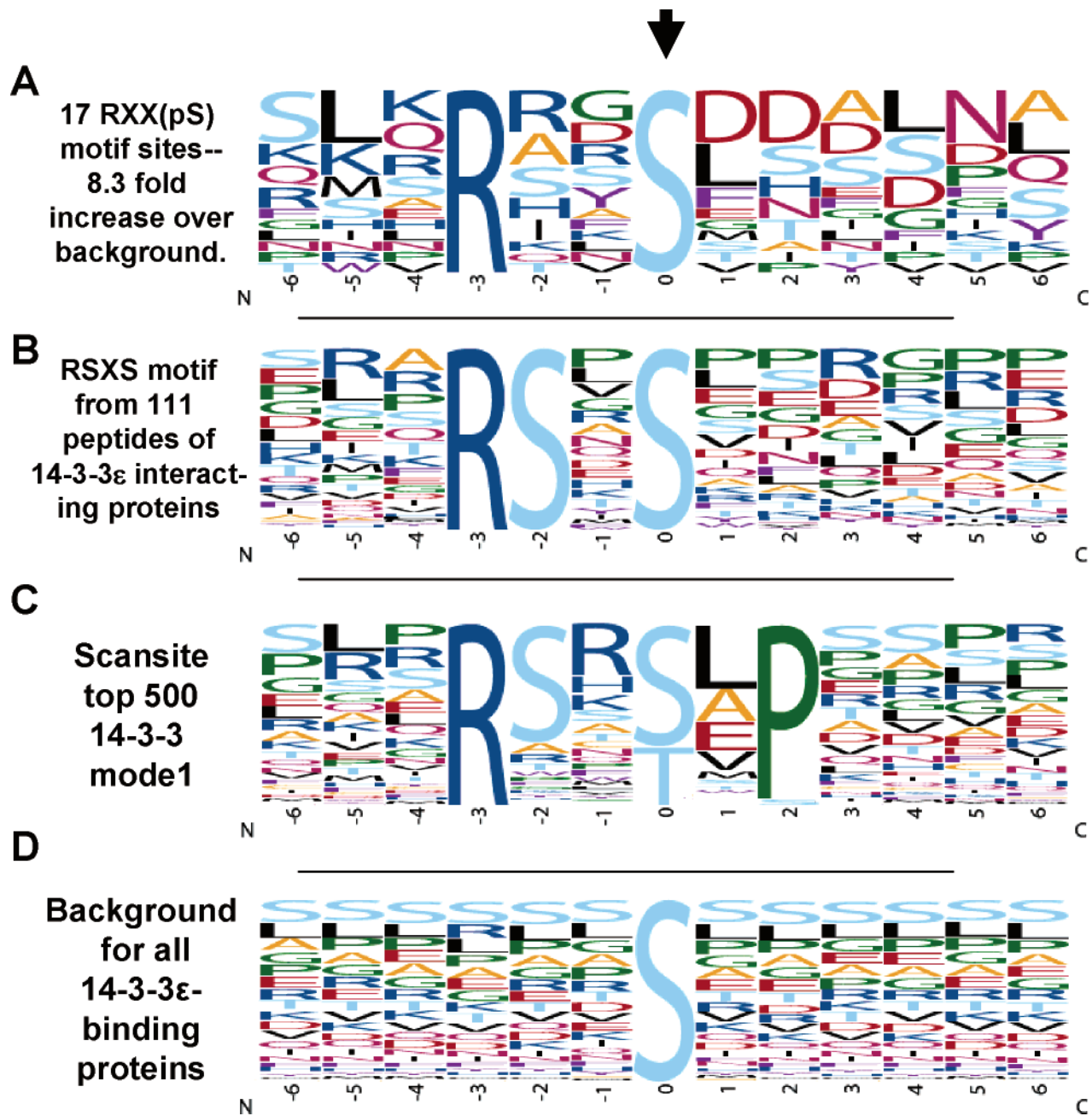


**Figure 3.** Phosphomotif analysis of identified proteins and phosphopeptides. (A) Frequency display of amino acids surrounding the motif (RXX(pS)) identified in 17 of the 60 unambiguously identified phosphorylation sites. The motif was identified using an iterative search algorithm (see Experimental Procedures for details). The RXX(pS) motif was found in the phosphorylation site data 8.3-fold higher than found in the mouse proteome. Letters spanning the entire height of the logo constitute the motif, and the height of each letter represents its relative abundance. (B and C) The primary structures of all identified 14-3-3ε interacting proteins were subjected to a sliding 13-mer division. All 13-mers were then compiled into one database. This database was subjected to the motif search analysis as in (A). A total of 111 peptides was identified containing the motif RSXS, and the frequency display of these peptides (B) shows great similarity to the frequency display (C) of the top 500 Scansite<sup>24</sup> mode1 14-3-3 interacting motifs in the mammalian Swiss-Prot database. (D) Frequency display for all 13-mers from the identified 14-3-3ε interacting proteins with one serine fixed shows no obvious bias over normal amino acid occurrence frequencies. The arrow indicates the position of the fixed serine residue in each frequency display.

results. Sequence logos representing the frequency of residues surrounding the central residue were created from the subset of sequences in the data set matching the given motif at the appropriate stage of the motif extraction procedure. All sequence logos were generated using the Weblogo software at <http://weblogo.berkeley.edu>.

## Results and Discussion

As 14-3-3 isoforms primarily bind to and regulate phosphoprotein substrates,<sup>10,22</sup> we employed a subtractive chromatography approach (Figure 1A) to enrich for phosphorylated 14-3-3ε substrates directly from embryonic murine brain extracts

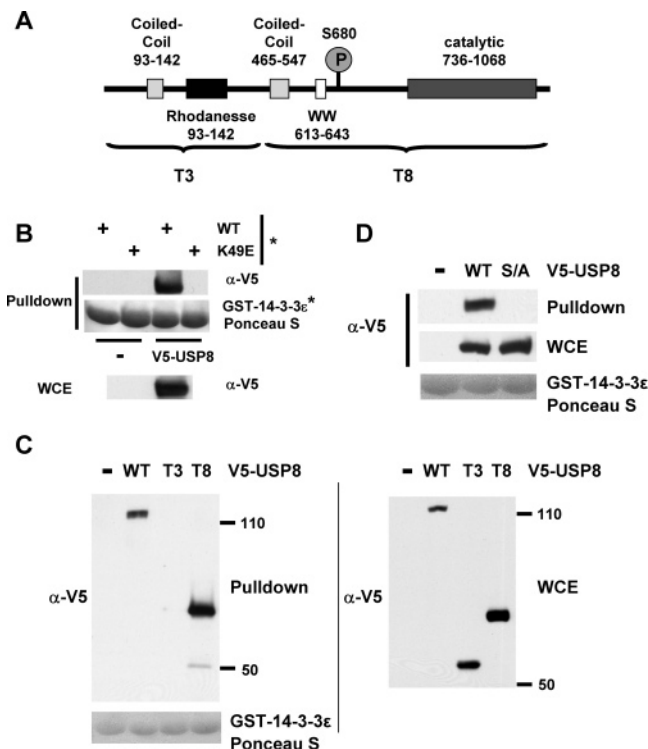


**Figure 4.** S680 of USP8 is required for its interaction with 14-3-3 $\epsilon$ . (A) Schematic of USP8 indicating the position of S680 relative to its known functional domains. The amino-terminal (T3) and carboxyl-terminal (T8) truncation mutants are indicated. (B) USP8 binds to wild-type and not USP8 (K49E). Cells were left untransfected or transfected with wild-type, V5-tagged USP8, and whole cell extracts (WCE) were subjected to GST-14-3-3 $\epsilon$  pull-down assays and immunoblot analysis using either wild-type or K49E GST-14-3-3 $\epsilon$  as indicated. Levels of GST-14-3-3 $\epsilon$  in each assay were visualized by Ponceau S. (C) 14-3-3 $\epsilon$  interacts with the carboxyl-terminal truncation mutant harboring S680 and not the amino-terminal truncation mutant. Cells were left untransfected or transfected with either full-length wild-type USP8 or truncation mutants T3 or T8. Whole cell extracts were subjected to GST-14-3-3 $\epsilon$  pull-down assays (left panel) and immunoblot analysis (right panel). Levels of GST-14-3-3 $\epsilon$  in each assay were visualized by Ponceau S (lower left panel). (D) Mutation of S680 to alanine abolishes its interaction with 14-3-3 $\epsilon$ . Transfections and analyses were performed as in (B) and (C).

as was used previously to identify phospho-dependent Dab1 interacting partners.<sup>5</sup> A total of 145 mg of embryonic day 16.5 combined forebrain and midbrain extract was pre-cleared over glutathione sepharose. GST-specific interactions were then subtracted over a column of glutathione sepharose bound to GST. Subtraction of phosphorylation-independent 14-3-3 $\epsilon$  interacting proteins was then performed by passing the extract over a GST-14-3-3 $\epsilon$  column harboring a K49E point mutation in the phosphoprotein binding cleft. This mutation renders 14-3-3 isoforms dramatically deficient in binding to phosphoprotein substrates.<sup>23</sup> The flow-through from this column was split equally, and half was passed again over a GST-14-3-3 $\epsilon$  K49E column, and the other half was applied to a column of wild-type GST-14-3-3 $\epsilon$ . After washing, proteins bound to the bait columns were eluted with MgCl<sub>2</sub>, precipitated with TCA, and subjected to SDS-PAGE and coomassie staining (Figure 1B). Significant amounts of coomassie staining, including many distinct bands, were present in the eluate from the wild-type column, and only minor signals were visible from the eluate

of the mutant column. Importantly, relatively little bait protein was observed in either eluate despite heavily and equally charged columns (Figure 1B, lower panel). To determine if potential 14-3-3 phosphoprotein substrates were enriched in the eluate from the wild-type column, 10 percent of the amount of eluates run for coomassie staining was subjected to immunoblotting with a motif-specific antibody which selectively recognizes many phosphorylation sites lying in the optimal model 14-3-3 general recognition sequence RSX(p[S/T])XP.<sup>9</sup> The wild-type eluate showed strong immunoreactivity and a number of distinct bands of variable intensity showing enrichment in phosphorylated 14-3-3 substrates (Figure 1C). However, the immunoblot did not reproduce the exact pattern seen in the coomassie stain, suggesting either the enrichment of nonphosphorylated 14-3-3 $\epsilon$  interacting proteins or 14-3-3 $\epsilon$  substrates whose phosphorylation sites did not fall in the canonical model recognition sequence. Nde11 binds 14-3-3 $\epsilon$  via three noncanonical phosphorylation sites.<sup>6</sup> To determine if Nde11 was present in our eluates, we immunoblotted for the presence of Nde11 and found it uniquely in the wild-type eluate (Figure 1C, lower panel). This suggested that the eluate from the wild-type 14-3-3 $\epsilon$  column was enriched for both canonical and nontraditional 14-3-3 $\epsilon$  binding proteins. Interestingly, the Nde11 bound to 14-3-3 $\epsilon$  was enriched in the decreased mobility (potentially phosphorylated) form relative to the predominant increased mobility form in whole brain extract.

To identify the proteins in the wild-type eluate, we cut the entire gel lane into 16 specific bands and 18 regions interspersed between the bands (Supporting Information Figure 1). Each was digested in-gel with trypsin, and extracted peptides were subjected to liquid chromatography–tandem mass spectrometry (LC–MS/MS). Mass spectra were interrogated by searching the mouse IPI database, and 163 unique proteins were identified that matched to at least two tryptic peptides. Results for each band and gel region are presented in Supporting Information Table 1. We also identified 65 specific phosphorylation sites and 20 more where the site could not be precisely located due to the plausibility of the spectra matching to an alternate serine or threonine residue in the same phosphopeptide. Each phosphopeptide is listed with its corresponding protein and gel band in Supporting Information Table 1. Supporting Information Tables 3 and 4 give the nonredundant lists of identified proteins and phosphorylation sites, respectively.

The 14-3-3 $\epsilon$  interacting proteins that we identified in this study from embryonic murine brain were compared to those identified from other large-scale studies, each of which used different 14-3-3 isoforms and immortalized human cell lines. Venn diagrams, Figure 2A–D, show the overlap of 14-3-3 $\epsilon$  interacting proteins and those found to interact with other 14-3-3 isoforms. The overlap between this and any one of the other studies ranged from 8 to 18% (Figure 2E). The overlap between this study and all of the other studies combined was 32%. This could be extended to 52% if related isoforms were also considered as overlapping. For example, we identified three isoforms of the Slit-Robo Rho GTPase activating Protein (srGAP) family, and these could be considered overlapping with the one isoform identified among the other studies. Supporting Information Table 5 provides a list of the 14-3-3 interacting proteins identified in each of the large-scale studies and served as the basis for the generation of the Venn diagrams in Figure 2.

A phosphorylation-dependent interaction with 14-3-3 $\epsilon$  would, by definition, require stoichiometric phosphorylation in the

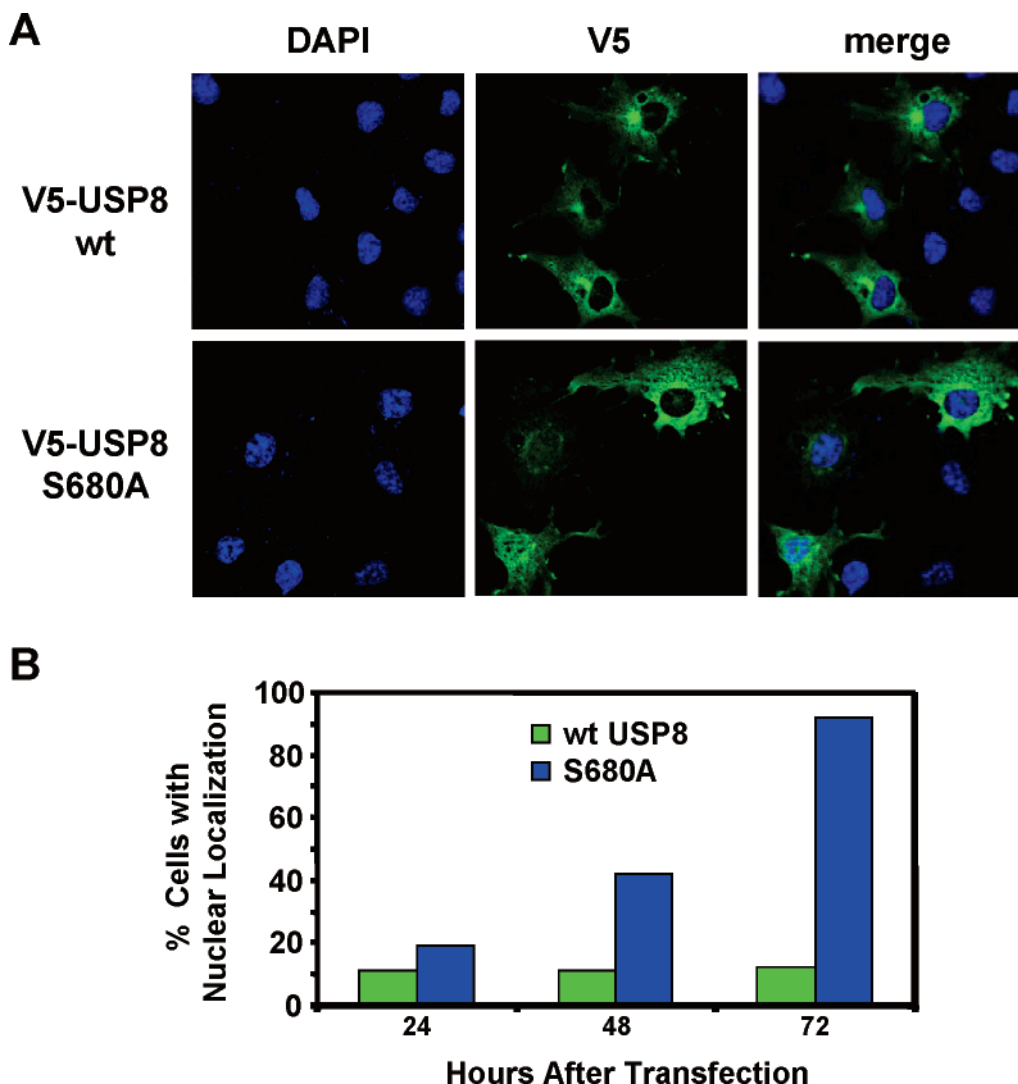


**Figure 5.** S680 governs the subcellular localization of the deubiquitinating enzyme USP8. COS-7 cells transfected with either wild-type (A, upper panels) or S680A (A, lower panels) V5-tagged USP8 constructs were analyzed for subcellular localization by immunofluorescence microscopy. The cells shown in (A) are from the 24 h time point and show the initial variability in USP8 S680A localization. Nuclei are stained with Dapi (blue), and USP8 is localized by anti-V5 immunofluorescence. (B) The percentage of cells showing V5-USP8 nuclear localization was quantified at 24, 48, and 72 h after transfection.

binding motif. We thus reasoned that on average we had an increased probability of identifying the phosphorylation sites required for binding to 14-3-3 $\epsilon$  on the interacting proteins relative to their total cellular pool. To determine if 14-3-3 binding motifs might be enriched in the phosphorylation sites we identified, we subjected all of the unambiguously identified serine phosphorylation sites to an iterative phosphomotif search algorithm (motif-x)<sup>21</sup> setting the motif identification threshold to 10 unique sequences. We identified two high complexity motifs that were found in this dataset at a significantly ( $P \leq 0.000001$ ) higher frequency than were found in the mouse proteome. These motifs were RXX(pS) (Figure 3A) and (pS)P (Supporting Information Figure 2B).

A visualization of the amino acid frequencies surrounding the 17 phosphorylation sites which contain the RXX(pS) motif (Figure 3A) looks similar to the preferred 14-3-3 model binding motif R(S/X)X(pS)XP.<sup>9</sup> As this motif analysis was dependent on identified phosphopeptides, we asked if motif interrogation using exclusively the sequences of the identified 14-3-3 $\epsilon$  interacting proteins might also reveal an increase in the relative

frequency of potential 14-3-3 binding sites. Our analysis found only one high complexity sequence motif (RSXS) of major significance ( $P \leq 0.000001$ ) from the sequences of the 14-3-3 $\epsilon$  interacting proteins. We visualized additional amino acid preferences occurring in this motif (Figure 3B) and found they were very similar to those in the model 14-3-3 binding motif which was visualized (Figure 3C) by employing Scansite<sup>24</sup> to extract the top 500 14-3-3 model sites in the mammalian Swiss-Prot database. Importantly, the relative abundance of each amino acid surrounding any fixed serine residue for the entire identified protein dataset showed little selectivity and roughly paralleled the amino acid frequencies in mammalian proteomes with serine and leucine as the most abundant amino acids (Figure 3D). Although we cannot exclude the possibility that some of the identified proteins interact with 14-3-3 $\epsilon$  nonspecifically or indirectly, the enrichment for phosphorylation-dependent interaction is evident not only by the phospho-14-3-3 substrate immunoblot shown in Figure 1B, but also by the increased frequency of potential 14-3-3 binding motifs in the identified proteins themselves. Ultimately, more targeted

analyses are required to fully define the nature of the interaction between the identified binding proteins and 14-3-3 $\epsilon$ . A particular emphasis will be placed on the participation of phosphorylated amino acids found in sequences resembling 14-3-3 binding motifs. However, strict compliance to the optimal binding motif is not always required, as a number of 14-3-3 binding partners have been identified that do not contain an optimal binding motif. Indeed it has been suggested that a lower affinity binding may be better suited for interactions requiring rapid on/off kinetics.<sup>10</sup>

Interestingly, of the 17 phosphopeptides that harbored the RXX(pS) motif, a manual examination of these identified phosphopeptides found only one phosphorylation site that fit exactly the optimal model 14-3-3 binding motif and is based on phosphoserine 680 in the deubiquitinating (DUB) enzyme USP8 (also known as UBPY). Of note, we previously identified USP8 phosphorylation at S680 in a phosphoproteomic analysis of embryonic mouse brain and predicted USP8 would bind to 14-3-3 isoforms.<sup>18</sup> To examine if S680 phosphorylation was required for the interaction with 14-3-3 $\epsilon$ , we transfected wild-type and mutant USP8 cDNA constructs into human embryonic kidney 293 cells for analysis in GST-14-3-3 $\epsilon$  pulldown assays. We first confirmed that wild-type but not 14-3-3 $\epsilon$  K49E bound to USP8 (Figure 4B). We also asked which region of USP8 bound 14-3-3 $\epsilon$  and found that the carboxyl-terminal and not the amino-terminal side of USP8 interacted with 14-3-3 $\epsilon$  (Figure 4C). Finally, mutation of serine 680 to alanine (S680A) completely abolished the interaction between USP8 and 14-3-3 $\epsilon$  (Figure 4D).

14-3-3 isoforms have been shown to regulate the subcellular localization of a number of phosphoprotein substrates,<sup>25</sup> and 14-3-3 $\epsilon$  specifically regulates the subcellular localization of Ndel1 and its binding partners LIS1 and cytoplasmic dynein.<sup>6</sup> We therefore asked if USP8 S680A would show altered subcellular localization. Indeed as shown in Figure 5, whereas wild-type USP8 remained primarily localized in the cytosol, USP8 S680A accumulated in the nucleus. Of the four large-scale 14-3-3 substrate studies in mammalian cells, Meek et al. and Benzinger et al. found the interaction of USP8 with 14-3-3 isoforms. Interestingly Meek et al. found this interaction in asynchronous and not mitotic HeLa cells, suggesting the interaction is cell cycle-regulated. Together, this suggests that a USP8 S680 kinase active in interphase may become inactivated sometime during G1 or M-phase. Alternatively, a USP8 phosphatase could become activated during G1 or M-phase and thereby reduce the interaction of USP8 with 14-3-3. DUB activity can protect a protein from proteasome-dependent degradation. Indeed, USP8 catalytic activity has recently been shown to stabilize the E3 ligase Nrdp1.<sup>17</sup> Given the stable interaction of USP8 and 14-3-3 in interphase, we find it an attractive model that USP8 would deubiquitinate and thereby stabilize negative regulators of the cell cycle that also bind 14-3-3 isoforms and might be brought to USP8 via 14-3-3 dimerization.<sup>10,12</sup> Such negative regulators of the cell cycle might include the tumor suppressors neurofibromin (NF1) and the Tuberous Sclerosis Complex proteins 1 and 2 (TSC1 and 2) which we found to interact with 14-3-3 $\epsilon$  and which have been found to undergo ubiquitin-dependent degradation.<sup>26,27</sup>

## Conclusion

Using a subtractive affinity chromatography approach to enrich for phospho-dependent interactions, we report here the first large-scale study of 14-3-3 $\epsilon$  interacting partners from

primary animal tissue. We identified 163 14-3-3 $\epsilon$  binding proteins from embryonic murine brain, where 14-3-3 $\epsilon$  has a genetically defined role. Roughly half of the identified 14-3-3 $\epsilon$  interacting proteins did not overlap with those identified in other large-scale proteomic experiments studying different 14-3-3 isoforms. This suggests we have identified 14-3-3 $\epsilon$ -specific substrates or 14-3-3 substrates that are phosphorylated and enriched in embryonic brain relative to the cell lines used in previous studies. We also report the first large dataset of phosphorylation sites from mammalian 14-3-3 interacting proteins and show that phosphorylation of one of these sites, serine 680 of USP8, is essential for a USP8–14-3-3 $\epsilon$  complex and directly regulates the subcellular localization of USP8. Taken together, these data offer a rich platform for more targeted studies of the roles played by 14-3-3 $\epsilon$  substrates during brain development.

**Acknowledgment.** We are grateful to M. Yaffe and S. Hirotsune for reagents and to F. McKeon for access to dissection equipment. This work was supported by National Institutes of Health Grants HG3456 (S.P.G.), GMG79452 (S.P.G.), and GM068994 (K.L.C.).

**Supporting Information Available:** Figures showing the gel band and regions that were subjected to LC–MS/MS analysis and an amino acid frequency plot showing the (pS)P motif; tables listing every identified phosphopeptide, protein, phosphorylation site, and 14-3-3 interacting proteins. This material is available free of charge via the Internet at <http://pubs.acs.org>.

## References

- May, P.; Herz, J.; Bock, H. H. Molecular mechanisms of lipoprotein receptor signalling. *Cell. Mol. Life Sci.* **2005**, *62*, 2325–2338.
- Feng, Y.; Walsh, C. A. Mitotic spindle regulation by Nde1 controls cerebral cortical size. *Neuron* **2004**, *44*, 279–293.
- Tissir, F.; Goffinet, A. M. Reelin and brain development. *Nat. Rev. Neurosci.* **2003**, *4*, 496–505.
- Nikolic, M. The molecular mystery of neuronal migration: FAK and Cdk5. *Trends Cell Biol.* **2004**, *14*, 1–5.
- Ballif, B. A.; Arnaud, L.; Arthur, W. T.; Guris, D.; Imamoto, A.; Cooper, J. A. Activation of a Dab1/CrkL/C3G/Rap1 pathway in Reelin-stimulated neurons. *Curr. Biol.* **2004**, *14*, 606–610.
- Toyo-oka, K.; Shionoya, A.; Gambello, M. J.; Cardoso, C.; Leventer, R.; Ward, H. L.; Ayala, R.; Tsai, L. H.; Dobyns, W.; Ledbetter, D.; Hirotsune, S.; Wynshaw-Boris, A. 14-3-3epsilon is important for neuronal migration by binding to NUDEL: a molecular explanation for Miller-Dieker syndrome. *Nat. Genet.* **2003**, *34*, 274–285.
- Shu, T.; Ayala, R.; Nguyen, M. D.; Xie, Z.; Gleeson, J. G.; Tsai, L. H. Ndel1 operates in a common pathway with LIS1 and cytoplasmic dynein to regulate cortical neuronal positioning. *Neuron* **2004**, *44*, 263–277.
- Tsai, L. H.; Gleeson, J. G. Nucleokinesis in neuronal migration. *Neuron* **2005**, *46*, 383–288.
- Yaffe, M. B.; Rittinger, K.; Volinia, S.; Caron, P. R.; Aitken, A.; Leffers, H.; Gambin, S. J.; Smerdon, S. J.; Cantley, L. C. The structural basis for 14-3-3: phosphopeptide binding specificity. *Cell* **1997**, *91*, 961–971.
- Bridges, D.; Moorhead, G. B. 14-3-3 proteins: a number of functions for a numbered protein. *Sci. STKE*, **2005**, 2005, re10.
- Cardoso, C.; Leventer, R. J.; Ward, H. L.; Toyo-Oka, K.; Chung, J.; Gross, A.; Martin, C. L.; Allanson, J.; Pilz, D. T.; Olney, A. H.; Mutchinick, O. M.; Hirotsune, S.; Wynshaw-Boris, A.; Dobyns, W. B.; Ledbetter, D. H. Refinement of a 400-kb critical region allows genotypic differentiation between isolated lissencephaly, Miller-Dieker syndrome, and other phenotypes secondary to deletions of 17p13.3. *Am. J. Hum. Genet.* **2003**, *72*, 918–930.
- Rushworth, L. K.; Hindley, A. D.; O'Neill, E.; Kolch, W. Regulation and role of Raf-1/B-Raf heterodimerization. *Mol. Cell. Biol.* **2006**, *26*, 2262–72.

- (13) Pozuelo Rubio, M.; Geraghty, K. M.; Wong, B. H.; Wood, N. T.; Campbell, D. G.; Morrice, N.; Mackintosh, C. 14-3-3-affinity purification of over 200 human phosphoproteins reveals new links to regulation of cellular metabolism, proliferation and trafficking. *Biochem. J.* **2004**, *379*, 395–408.
- (14) Meek, S. E.; Lane, W. S.; Piwnica-Worms, H. Comprehensive proteomic analysis of interphase and mitotic 14-3-3-binding proteins. *J. Biol. Chem.* **2004**, *279*, 32046–32054.
- (15) Jin, J.; Smith, F. D.; Stark, C.; Wells, C. D.; Fawcett, J. P.; Kulkarni, S.; Metalnikov, P.; O'Donnell, P.; Taylor, P.; Taylor, L.; Zougman, A.; Woodgett, J. R.; Langeberg, L. K.; Scott, J. D.; Pawson, T. Proteomic, functional, and domain-based analysis of in vivo 14-3-3 binding proteins involved in cytoskeletal regulation and cellular organization. *Curr. Biol.* **2004**, *14*, 1436–1450.
- (16) Benzinger, A.; Muster, N.; Koch, H. B.; Yates, J. R., III; Hermeking, H. Targeted proteomic analysis of 14-3-3 sigma, a p53 effector commonly silenced in cancer. *Mol. Cell. Proteomics* **2005**, *4*, 785–795.
- (17) Wu, X.; Yen, L.; Irwin, L.; Sweeney, C.; Carraway, K. L., III. Stabilization of the E3 ubiquitin ligase Nrdp1 by the deubiquitinating enzyme USP8. *Mol. Cell. Biol.* **2004**, *24*, 7748–7757.
- (18) Ballif, B. A.; Villen, J.; Beausoleil, S. A.; Schwartz, D.; Gygi, S. P. Phosphoproteomic analysis of the developing mouse brain. *Mol. Cell. Proteomics* **2004**, *3*, 1093–1101.
- (19) Elias, J. E.; Haas, W.; Faherty, B. K.; Gygi, S. P. Comparative evaluation of mass spectrometry platforms used in large-scale proteomics investigations. *Nat. Methods* **2005**, *2*, 667–675.
- (20) Diamonti, A. J.; Guy, P. M.; Ivanof, C.; Wong, K.; Sweeney, C.; Carraway, K. L., III. An RBCC protein implicated in maintenance of steady-state neuregulin receptor levels. *Proc. Natl. Acad. Sci. U.S.A.* **2002**, *99*, 2866–2871.
- (21) Schwartz, D.; Gygi, S. P. An iterative statistical approach to the identification of protein phosphorylation motifs from large-scale data sets. *Nat. Biotechnol.* **2005**, *23*, 1391–1398.
- (22) Yaffe, M. B. Master of all things phosphorylated. *Biochem. J.* **2004**, *379*, e1–2.
- (23) Zhang, L.; Wang, H.; Liu, D.; Liddington, R.; Fu, H. Raf-1 kinase and exoenzyme S interact with 14-3-3zeta through a common site involving lysine 49. *J. Biol. Chem.* **1997**, *272*, 13717–13724.
- (24) Obenaus, J. C.; Cantley, L. C.; Yaffe, M. B. Scansite 2.0: Proteome-wide prediction of cell signaling interactions using short sequence motifs. *Nucleic Acids Res.* **2003**, *31*, 3635–3641.
- (25) Dougherty, M. K.; Morrison, D. K. Unlocking the code of 14-3-3. *J. Cell Sci.* **2004**, *117*, 1875–84.
- (26) Cichowski, K.; Santiago, S.; Jardim, M.; Johnson, B. W.; Jacks, T. Dynamic regulation of the Ras pathway via proteolysis of the NF1 tumor suppressor. *Genes Dev.* **2003**, *17*, 449–454.
- (27) Plas, D. R.; Thompson, C. B. Akt activation promotes degradation of tuberlin and FOXO3a via the proteasome. *J. Biol. Chem.* **2003**, *278*, 12361–12366.

PR060206K